Case Report

Computed tomography and magnetic resonance imaging of maxillofacial rhabdomyosarcoma and suspected multiple metastases including the epidural space and bone marrow in a dog

Sang-Kwon Lee[1] Seulgi Bae[2] Min Jang[3] Kija Lee[1*]

Abstract

A 3-year-old mixed-breed dog presenting with a recurrent maxillofacial tumor was diagnosed with recurrent rhabdomyosarcoma. Computed tomography and magnetic resonance imaging revealed a left maxillofacial mass, left cervical lymph node enlargement, epidural mass dorsal to the 6th lumbar vertebra compressing the cauda equina, soft-tissue mass ventral to the 6th lumbar vertebra, multiple subcutaneous nodules and signal changes in the paravertebral muscles. The left maxilla, lumbar spine and ilium exhibited diffuse signal changes and contrast enhancement upon magnetic resonance imaging. This is, to our knowledge, the first reported case of bone marrow and epidural-space involvement of a canine rhabdomyosarcoma.

Keywords: bone marrow infiltration, canine, juvenile, soft tissue sarcoma, spine

[1]*Department of Veterinary Medical Imaging, College of Veterinary Medicine, Kyungpook National University, Daegu 41566, Republic of Korea*

[2]*Department of Veterinary Internal Medicine, College of Veterinary Medicine, Kyungpook National University, Daegu 41566, Republic of Korea*

[3]*Department of Veterinary Surgery, College of Veterinary Medicine, Kyungpook National University, Daegu 41566, Republic of Korea*

****Correspondence:*** *leekj@knu.ac.kr* (K. Lee)

Received: March 5, 2023
Accepted: May 23, 2023
https://doi.org/10.14456/tjvm.2023.34

Introduction

Rhabdomyosarcomas (RMS) is a rare tumor in dogs, most commonly occurring in the head and neck (Chang H-W *et al*., 2006; Scott EM *et al*., 2016; Connell DR *et al*., 2020). RMS have high metastasis rates and the most common metastatic sites are known to be the lung and lymph nodes (Connell DR *et al*., 2020). However, only a limited number of cases have been reported in veterinary medicine. Most previous report on RMS in dogs has been focused on clinical and histopathological findings and a detailed description of the imaging features of RMS is lacking.

This case report introduces a case with suspected metastasis to the lymph nodes, epidural space, bone marrow, paravertebral muscle and subcutaneous tissue in a dog diagnosed with maxillofacial RMS. In this report, we described the computed tomography (CT) and magnetic resonance imaging (MRI) features of maxillofacial RMS and the challenge point of the interpretation of the signal changes in bone marrow in MRI when cortical bone lysis is not accompanied by CT.

Case description

A 3-year-old, 14.5-kg, male, mixed-breed dog presented with a recurrent left maxillofacial mass, dysuria, dyschezia and exercise intolerance. Five months prior, the dog underwent enucleation and removal of the left maxillofacial mass, which was diagnosed as an embryonal RMS based on histology and immunohistochemistry. One month previously whole-body CT and lumbar MRI were performed to evaluate the recurrent maxillofacial mass and hind-limb lameness; MRI revealed an epidural mass at the 6th lumbar vertebra. At presentation, a firm mass was observed in the left maxillofacial region. The proprioceptive reaction was decreased in both hindlimbs and the dog exhibited lumbar back pain.

Abdominal and thoracic radiographic characteristics were unremarkable. CT and MRI were performed with the patient under general anesthesia. General anesthesia was induced using intravenous butorphanol (0.2 mg/kg), midazolam (0.2 mg/kg) and propofol (5 mg/kg) and maintained with isoflurane (1.5%–2.5%) and oxygen (1 L/min) after endotracheal intubation.

CT was performed using a 16-channel multi-detector CT scanner (Alexion; Canon Medical Systems, Tokyo, Japan). The scanning parameters were as follows: 120 kV, 110 mA, and 1-mm thickness. The dog was positioned in sternal recumbency and whole-body CT images were obtained before and after 2 ml/kg of iohexol injection (Bonorex 300; Daihan Pharm, Korea). For head CT, images were obtained for two early phases (10 and 30 s after contrast injection) and a delayed phase (90 s) and only a delayed-phase (120 s) image was obtained for thoracic and abdominal CT. Thereafter, MRI was performed using a 1.5-tesla MRI system (GE Signa Explorer; GE Healthcare, Korea). The dog was positioned in dorsal recumbency and head and lumbar images were obtained using an 8-channel knee coil and 16-channel flexible coil, respectively. The following sequences were used: T2-weighted image (T2WI), T1-weighted image (T1WI), short-tau inversion recovery (STIR), diffusion-weighted image (DWI) and post-contrast T1WI with or without fat suppression (FS).

Head CT and MRI revealed a soft-tissue mass in the left infraorbital lesion (Fig. 1). Upon CT, it was slightly hypoattenuating to the muscle, with mild, heterogeneous contrast enhancement. Upon MRI, the mass was hyperintense via T2WI and STIR and isointense via T1WI compared to the muscle, with mild, heterogeneous contrast enhancement. It exhibited a restrictive pattern upon DWI and apparent diffusion coefficient mapping. CT revealed lysis of the adjacent body and zygomatic process of the maxilla. Although the remaining left maxilla did not exhibit distinct changes upon CT, it exhibited diffuse hyperintensity upon MRI of the left maxilla via T2WI and STIR, an intermediate signal via T1WI and mild contrast enhancement (Fig. 2). Enlargement of the left medial retropharyngeal and parotid lymph nodes was observed upon CT and MRI.

Lumbar CT and MRI revealed broad-based masses on the dorsal and ventral surfaces of the 6th lumbar (Figs. 3 and 4). The masses were isoattenuating or slightly hypoattenuating to the muscle, with relatively uniform contrast enhancement upon CT. Upon MRI, they were hyperintense to the muscle via T2WI, DWI, and STIR; isointense via T1WI; and exhibited moderate contrast enhancement. The cauda equina was severely compressed by the dorsal epidural mass. The thoracic and lumbar spine and both ilia exhibited diffusely heterogeneous signals via T2WI, STIR, and T1WI and heterogeneous hyperintensity via DWI. Post-contrast T1WI/FS images revealed heterogeneous enhancement of the lumbar vertebral body and ilium. Upon CT, diffuse and subtle decreases in density were observed throughout the lumbar vertebrae. Subcutaneous nodules were observed throughout the body, particularly at the caudal and lumbar level (Fig. 4). Although no distinct signal changes were observed via T1WI and T2WI, certain paravertebral muscles at the caudal and lumbar vertebrae exhibited strong enhancement compared with other muscles upon MRI (Fig. 4).

Compared with the CT and MRI examinations performed a month prior to presentation, the left maxillofacial mass and the epidural mass at the 6th lumbar slightly increased in size. Marked signal changes in the lumbar vertebrae, multiple subcutaneous nodules and paravertebral muscles were also observed. Considering the patient's history and progression of the lesions, recurrent maxillofacial RMS with metastasis to the lymph nodes, epidural space, bone marrow, paravertebral muscles and subcutaneous tissues was suspected. The dog was euthanized and no necropsy was performed, at the owner's request.

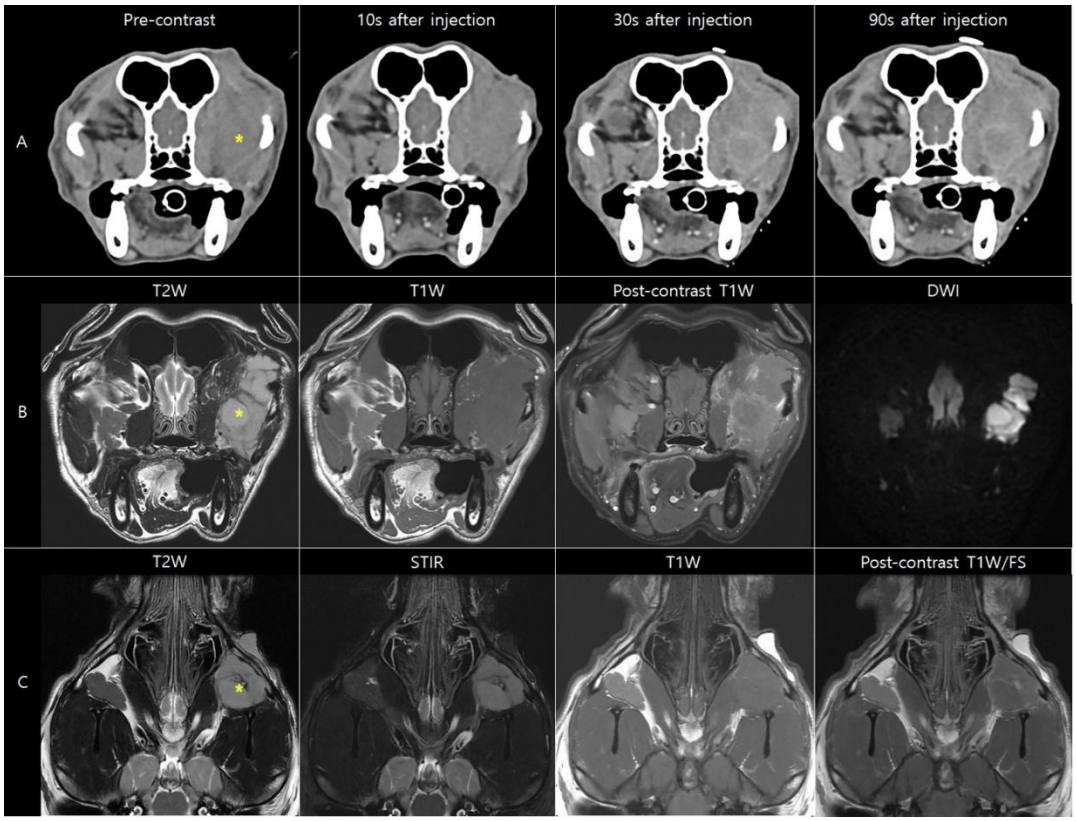

Figure 1 Transverse A, CT and B, MRI and C, dorsal MRI of the left maxillofacial canine rhabdomyosarcoma. Compared to the muscle, the mass (asterisk) is hypoattenuated upon CT; hyperintense upon T2-weighted imaging, short tau inversion recovery and diffusion-weighted imaging; and isointense upon T1-weighted imaging. The mass exhibited heterogeneous and mild contrast enhancement. CT, computed tomography; MRI, magnetic resonance imaging

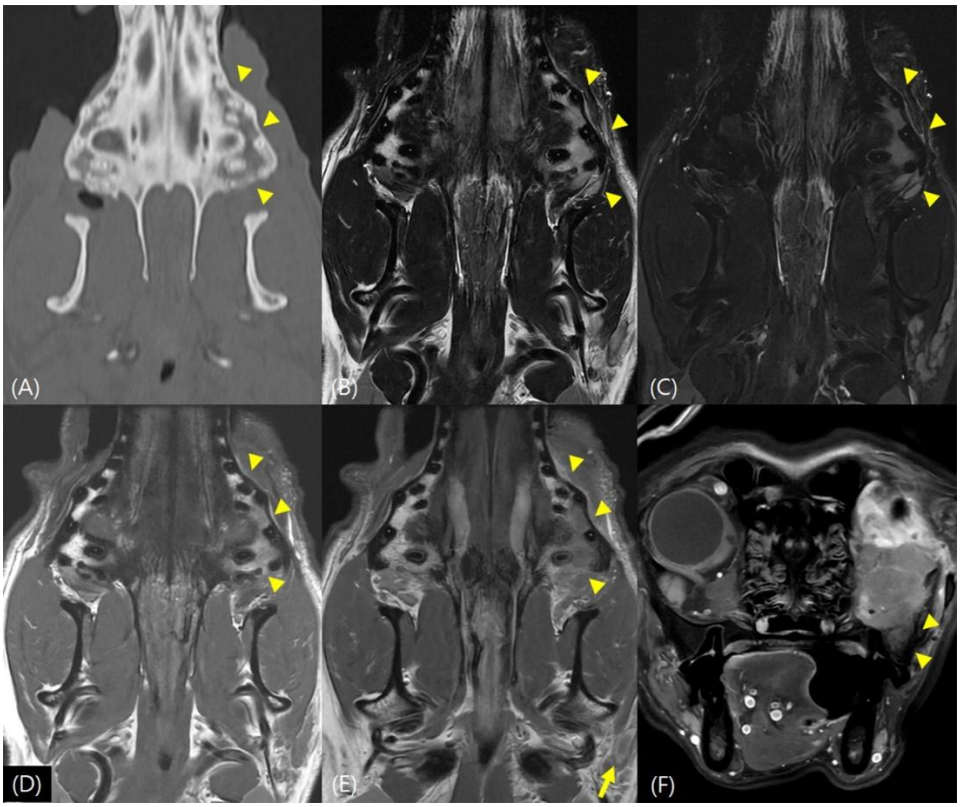

Figure 2 Dorsal-plane bone-window-reconstructed A, pre-contrast CT, B, T2WI, C, STIR, D, T1WI, and E, post-contrast T1WI and F, transverse post-contrast T1WI/fat-suppressed imaging. The left maxilla (arrowheads) does not exhibit a distinct change upon CT, but, upon MRI, it exhibits hyperintensity via T2WI and STIR and hypointensity via T1WI compared to the right maxilla as well as contrast enhancement. The left parotid lymph node is enlarged (arrow). CT, computed tomography; STIR, short tau inversion recovery; T1WI, T1-weighted imaging; T2WI, T2-weighted imaging

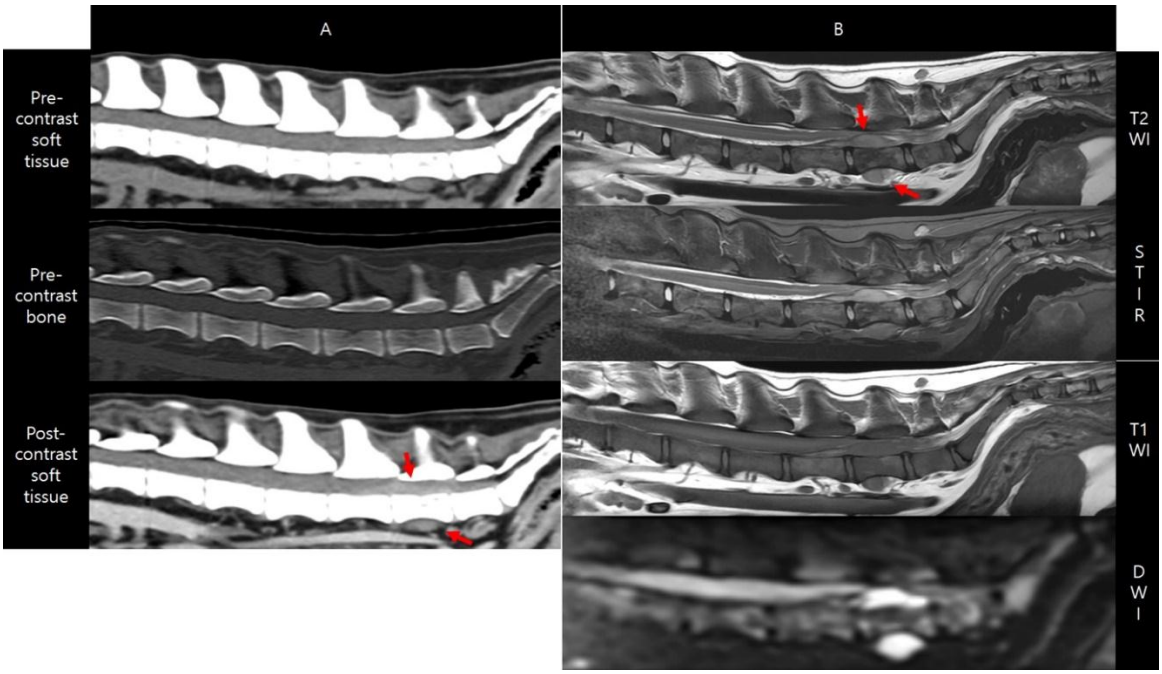

Figure 3 Sagittal-plane lumbar A, CT and B, MRI. Broad-based masses on the dorsal and ventral surface of the 6th lumbar vertebra (arrows). They are isoattenuating to the muscle and exhibit uniform contrast enhancement upon CT. Upon MRI, compared to the muscle, the masses are homogeneously hyperintense via T2WI and STIR, isointense via T1WI and hyperintense via DWI. A slightly decreased density of lumbar vertebral bodies is observed upon CT. Upon MRI, lumbar vertebral bodies are diffusely heterogeneous via T2WI, STIR and T1WI and heterogeneously hyperintense via DWI. CT, computed tomography; diffusion-weighted imaging, DWI; STIR, short tau inversion recovery; T1WI, T1-weighted imaging; T2WI, T2-weighted imaging

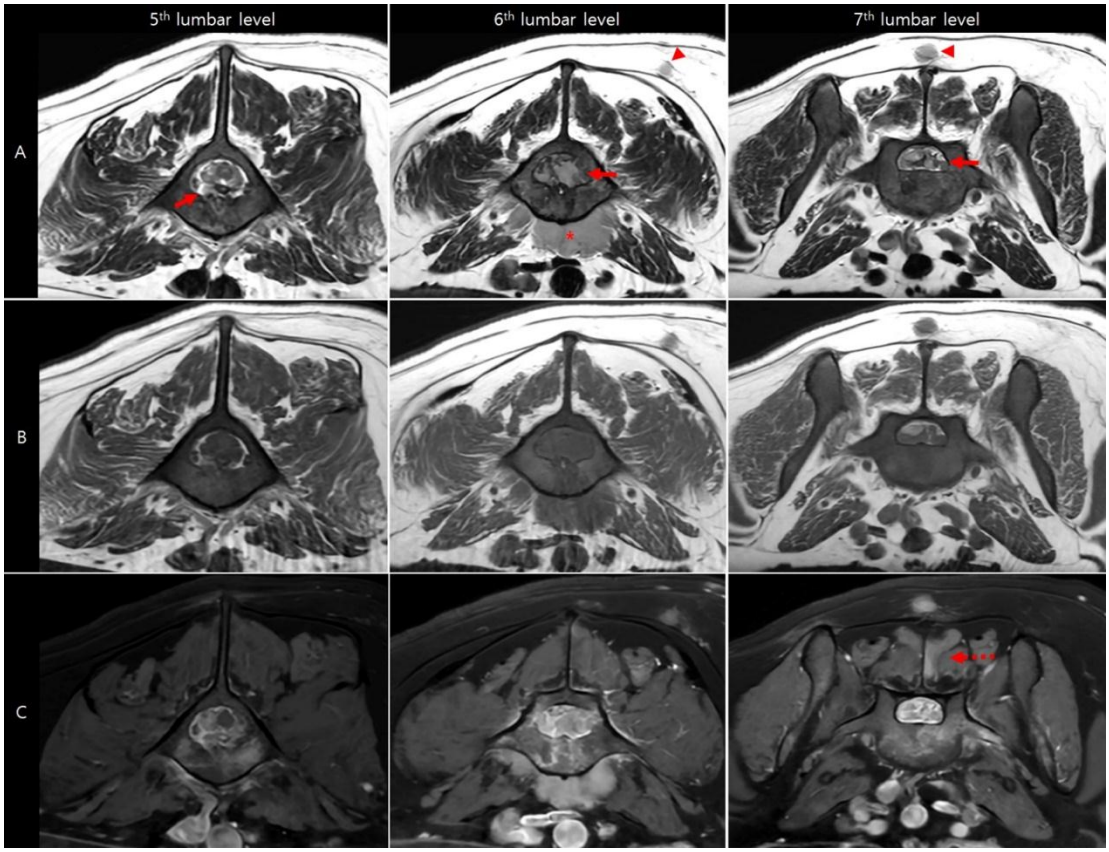

Figure 4 Transverse A–C, T2WI, D–F, T1WI and G–I, post-contrast T1WI/fat-suppressed images at L5–7. The epidural mass (arrows) is heterogeneously hyperintense to the muscle via T2WI, isointense via T1WI, and heterogeneously contrast-enhanced. The ventral aspect of the 6th lumbar vertebra exhibits a broad-based mass with a similar signal change to the epidural mass (asterisk). The lumbar spine exhibits a heterogeneous signal change via T2WI and T1WI as well as heterogeneous contrast enhancement. Subcutaneous nodules (arrowhead) and contrast enhancement of the paravertebral muscle (dashed arrow) are observed. T1WI, T1-weighted imaging; T2WI, T2-weighted imaging

Discussion

Herein, this case report describes the imaging features of recurrent maxillofacial RMS and suspected multiple metastases, including the lymph nodes, epidural space, bone marrow, paravertebral muscle and subcutaneous tissue. To our knowledge, this is the first detailed account of imaging features of this condition and the first case of suspected bone marrow and epidural metastasis of RMS in a dog.

RMSs are rare tumors in dogs. Although it has been reported in various ages, most frequently reported in dogs younger than 2 years (Chang H-W *et al*., 2006; Pinto da Cunha N *et al*., 2010; Scott EM *et al*., 2016; Gillem JM *et al*., 2018; Bailey KA *et al*., 2020). Diagnosis of RMS is based on the histopathology and immunohistochemistry of skeletal muscle specific-markers such as vimentin and desmin. They can be histologically classified as embryonal, botryoid, alveolar and pleomorphic. Alveolar and embryonal RMS have been most commonly reported in the subcutaneous, head and neck, with embryonal RMS being the most common subtype of canine orbital RMS (Scott EM *et al*., 2016). Most botryoid RMS in dogs has occurred in the urinary bladder and pleomorphic is the rarest type of RMS in dogs. In this case, embryonal RMS, diagnosed based on histology and immunohistochemistry, occurred in the maxillofacial region of a young dog.

RMS is considered very aggressive, with high metastasis and recurrence rates (Scott EM *et al*., 2016; Connell DR *et al*., 2020), with higher metastatic rate and shorter survival time compared to other soft tissue sarcomas in dogs (Caserto BG, 2013). In humans, alveolar RMS is considered to have more aggressive behavior and poor prognosis than embryonal RMS and botryoid RMS has a relatively favorable prognosis (Caserto BG, 2013). Similarly, in a previous review paper in dogs, alveolar and embryonal RMS had a higher metastatic rate (50%) than botryoid RMS (27%) (Caserto BG, 2013). However, due to their rarity and limited case numbers, the exact prognosis and metastatic rate of canine RMS according to histological subtype are unclear. Regardless of the histological type, the most common metastatic sites of canine RMS were the lymph nodes and lungs (Caserto BG, 2013; Connell DR *et al*., 2020; Scott Em *et al*., 2016). Other metastatic sites included various abdominal organs, subcutis, omentum and mesentery. (Caserto BG, 2013; Connell DR *et al*., 2020). In this case, although no histopathological examination was performed, metastases to the lymph nodes, epidural space, bone marrow, paravertebral muscle and subcutaneous tissue were suspected based on the patient's history and imaging characteristics. To our knowledge, in veterinary medicine, epidural metastasis of RMS has only been reported in a cat and no reports have described bone marrow metastasis of RMS. However, the bone marrow is a common metastatic site of human RMS; approximately 20% of patients have metastatic lesions at diagnosis, 30% of which involve the bone marrow (Bailey KA and Weexler LH, 2020; Huang C *et al*., 2021).

A detailed description of imaging features of canine RMS is lacking (Suzuki K *et al*., 2006; Gillem JM *et al*., 2018). In a case report of canine vaginal RMS, no information was provided on MRI signal changes (Suzuki K *et al*., 2006). In the present case, compared to the muscle, all lesions except that in the bone marrow were isoattenuating or slightly hypoattenuating upon pre-contrast CT, isointense via T1WI, and hyperintense via T2WI and STIR and exhibited restricted diffusion via DWI and heterogeneous contrast enhancement upon CT and MRI. Some of the CT and MRI imaging features of human orbital RMS are reportedly similar to those in the present case (Freling NJ *et al*., 2010; Zuh J *et al*., 2014). Although comparison in CT and MRI features between rhabdomyosarcoma and other soft tissue sarcomas in dogs is difficult due to the lack of studies and a single case of the present report, reported CT features of soft tissue sarcoma were similar to this case (Farmer RJ *et al*., 2023). In humans, reported imaging characteristics of RMS vary, possibly owing to the grade and histological type of RMS, and imaging features that differentiate RMS from other soft-tissue tumors have not been reported even in humans (Freling NJ *et al*., 2010; Zuh J *et al*., 2014).

Unlike the epidural mass and subcutaneous nodules, the suspected bone marrow metastasis did not resemble a mass or nodule in this case. Although MRI has not been routinely used for bone marrow evaluation in veterinary medicine, as we did here, it is considered the gold standard imaging modality for such cases in human medicine (Hwang S and Panicek DM, 2007; Shah LM and Hanrahan CJ, 2011). In humans, compared to the adjacent muscle or intervertebral disk, hypointense lesions in the bone marrow via T1WI are highly accurate indications of bone marrow abnormalities. Upon T2WI, a halo sign characterized by a hyperintense rim or diffuse hyperintensity is indicative of metastatic disease (Hwang S and Panicek DM, 2007; Shah LM and Hanrahan CJ, 2011). Upon fat-saturated T2WI or STIR MRI, most bone marrow pathologies exhibit high signal intensity. Bone marrow tumors also usually exhibit high signal intensity via DWI owing to their high cellularity (Hwang S and Panicek DM, 2007). Contrast-enhanced imaging enables the detection of enhancing metastatic lesions. Similarly, in this case, the lumbar vertebrae exhibited diffuse and heterogeneous hypointensity via T1WI; heterogeneous hyperintensity via T2WI, STIR, and DWI; and heterogeneous and marked contrast enhancement. Therefore, the patient was tentatively diagnosed with bone marrow metastasis of RMS.

During evaluation of bone marrow signal changes via MRI, pathological and physiological signal changes must be distinguished. Despite the absence of studies on MRI signal changes in the bone marrow in veterinary medicine, various signal changes have been reported in humans depending on the patient's age, sex and environment (Shah LM and Hanrahan CJ, 2011; Małkiewicz A and Dziedzic M, 2012; Shigematsu Y *et al*., 2014). The bone marrow consists of yellow (mostly fat) and red (containing hematopoietic cells) marrow. Yellow marrow exhibits a high and red marrow a low signal intensity via T1WI and T2WI. The signal intensity of bone marrow is determined by the distribution of yellow and red marrow, resulting in a mixed signal intensity according to their ratio,

especially during conversion or reconversion (Shah LM and Hanrahan CJ, 2011). However, signal changes due to conversion or reconversion typically appear homogeneous or patchy (Shah LM and Hanrahan CJ, 2011; Małkiewicz A and Dziedzic M, 2012; Shigematsu Y *et al*., 2014). In this case, signal changes in bone marrow were markedly heterogeneous, different to those of normal yellow or red marrow. Therefore, we do not consider the bone marrow signal change a physiological change.

In conclusion, we report the detailed CT and MRI features of maxillofacial RMS with suspected multiple metastases in a dog. This is, to our knowledge, the first reported case of bone marrow and epidural-space involvement of canine RMS.

Acknowledgements

This research was supported by the National Research Foundation of Korea (NRF) grant funded by the Korean Ministry of Science and ICT (2022R1G1A1006476).

References

Avallone G, Pinto da Cunha N, Palmieri C, Della Salda L, Stefanello D, Roccabianca P and Caniatti M 2010. Subcutaneous embryonal rhabdomyosarcoma in a dog. Vet Clin Pathol. 39: 499-504.

Bailey KA and Wexler LH 2020. Pediatric rhabdomyosarcoma with bone marrow metastasis. Pediatr Blood Cancer. 67: e28219.

Caserto BG 2013. A comparative review of canind and human rhabdomyosarcoma with emphasis on classification and pthogenesis. Vet Pathol. 50: 806-826.

Chang H-W, Ho S-Y, Lo H-F, Tu Y-C, Jeng C-R, Liu C-H, Wang F-I and Pang VF 2006. Vaccine-associated rhabdomyosarcoma with spinal epidural invasion and pulmonary metastasis in a cat. Vet Pathol. 43: 55-58.

Connell DR, Rodriguez Jr CO, Sternberg RA, Singh K, Barger A and Garrett LD 2020. Biological behaviour and ezrin expression in canine rhabdomyosarcomas: 25 cases (1990-2012). Vet Comp Oncol. 18: 675-682.

Farmer RJ, Poirier VJ, Nykamp S, Jensen M, Foster RA, Oblak M and Appleby R 2023. CT features of subcutaneous, intermuscular, and intramuscular mast cell tumors in dogs. Vet Raiol Ultrasound. 64: 53-60

Freling NJ, Merks JH, Saeed P, Balm AJ, Bras J, Pieters BR, Adam J and Rijn RR 2010. Imaging findings in craniofacial childhood rhabdomyosarcoma. Pediatr Radiol. 40: 1723-1738.

Gillem JM, Sullivan L and Sorenmo KU 2018. Diagnosis and multimodal treatment of metastatic maxillofacial juvenile embryonal rhabdomyosarcoma in a young golden retriever. J Am Anim Hosp Assoc. 54:e54505.

Huang C, Jian B, Su Y, Xu N, Yu T, He L, Zhang X, Liu Y, Jin M and Ma X 2021. Clinical features and prognosis of paediatric rhabdomyosarcoma with bone marrow metastasis: a single Centre experiences in China. BMC Pediatr. 21: 1-8.

Hwang S and Panicek DM 2007. Magnetic resonance imaging of bone marrow in oncology, Part 1. Skeletal Radiol. 36: 913-920.

Małkiewicz A and Dziedzic M 2012. Bone marrow reconversion: imaging of physiological changes in bone marrow. Pol J Radiol. 77: 45-50

Scott EM, Teixeira LB, Flanders DJ, Dubielzig RR and McLellan GJ 2016. Canine orbital rhabdomyosarcoma: a report of 18 cases. Vet Ophthalmol. 19: 130-137.

Shah LM and Hanrahan CJ 2011. MRI of spinal bone marrow: part 1, techniques and normal age-related appearances. AJR Am J Roentgenol. 197: 1298-1308.

Shigematsu Y, Hirai T, Kawanaka K, Shiraishi S, Yoshida M, Kitajima M, Uetani H, Azuma M, Iryo Y and Yamashita Y 2014. Distinguishing imaging features between spinal hyperplastic hematopoietic bone marrow and bone metastasis. AJNR AM J Neuroradiol. 35: 2013-2020.

Suzuki K, Nakatani K, Shibuya H and Sato T 2006. Vaginal rhabdomyosarcoma in a dog. Vet Pathol. 43: 186-188.

Zhu J, Zhang J, Tang G, Hu S, Zhou G, Liu Y, Dai L and Wang Z 2014. Computed tomography and magnetic resonance imaging observations of rhabdomyosarcoma in the head and neck. Oncol Lett. 8: 155-160.